Survey design for coal-scale 3D-PS seismic reflection

Shaun Strong[*] [†] *and Steve Hearn*[*] [†]

ABSTRACT

Survey design for converted-wave (PS) reflection is more complicated than for standard P-wave surveys, due to ray-path asymmetry and increased possibility of phase distortion. Coal-scale PS surveys (depth $<$ 300m) require particular consideration, partly due to the particular physical properties of the target (low density and low velocity). Finite-difference modeling provides a pragmatic evaluation of the likely distortion due to inclusion of post-critical reflections. If the offset range is carefully chosen then it may be possible to incorporate high-amplitude post-critical reflections without seriously degrading the resolution in the stack. Offsets of up to three times target depth may in some cases be usable, with appropriate quality control at the data-processing stage. This means that the PS survey design may need to handle ray paths which are highly asymmetrical, and which are very sensitive to assumed velocities.

A 3D-PS design case study is included for a particular coal survey with target in the depth range 85-140m. The objectives were acceptable fold balance between bins, and relatively smooth distribution of offset and azimuth within bins. These parameters are relatively robust for the P-wave design, but much more sensitive for the case of PS. Reduction of the source density is more acceptable than reduction of receiver density, particularly in terms of offset-azimuth distribution. This is a fortuitous observation in that it improves the economics of a dynamite source, which is desirable for high-resolution coal-mine planning.

The final survey design necessarily allowed for logistical and economic considerations, which implied some technical compromise. Nevertheless good fold, offset and azimuth distributions were achieved across the survey area, yielding a dataset suitable for meaningful analysis of P and S azimuthal anisotropy.

INTRODUCTION

Motivation for this study

The integration of conventional P-wave and PS-wave (converted, or C-wave) reflection can improve the characterization of the subsurface. This has been demonstrated for particular petroleum-scale targets, both offshore (e.g. Barkved et al., 1999; Hanson et al., 1999) and onshore (e.g. Dufour et al., 2002). More recently it has been demonstrated that the advantages of integrated P/PS reflection may also apply for shallower targets (e.g. coal, coal seam gas (CSG), hard-rock). In particular, integrated 2D P and PS imagery has been

[*] Velseis Pty Ltd, Brisbane, Australia
[†] School of Earth Sciences, University of Queensland, Brisbane, Australia.

shown to yield improved detection of fault structures and geometries, and provide superior imaging of the top-of-coal for shallow open-cut targets (e.g. Hearn, 2004; Hendrick, 2006).

For P-wave coal exploration, 3D surveys are now relatively common, providing detailed spatial interpretation critical for mine planning. As a logical extension to these trends, a recent trial (Strong and Hearn, 2011) has examined the feasibility and value of a 3D-3C survey over a coal target previously explored using 2D P-wave seismic and limited drilling. The overall objectives were to optimize 3D acquisition and processing of integrated P and PS data at the coal scale. The project included an in-depth investigation of survey design. The main purpose of this paper is to examine particular aspects of PS survey design which may require special attention in the case of coal-scale surveys (0-300m).

3D Survey Design

The broad aim of seismic survey design is to ensure that source and receiver configurations are optimized to give the best possible interpretation of the structures at the target horizons while satisfying logistical and economic constraints.

The subject of correct 3D survey design has been widely researched, particularly in the context of P-wave reflection (e.g. Liner and Underwood, 1999; Cooper, 2004). An even fold distribution is desirable in all reflection surveys. In 3D surveys an even distribution of azimuths and offsets within any bin is desirable particularly where azimuthal analysis is envisaged, including processing via common offset vector (COV) approaches (Vermeer, 1998; Cary, 1999). A poor distribution can result in reduced resolution, suboptimal processing, and noise artefacts including acquisition footprint. These may have a significant impact on the quality of the prestack migration (Gardner and Canning, 1994; Chemingui and Biondi, 1996). This can lead to misinterpretation of geological structures and can mask real azimuthal anisotropy. Migration algorithms have been developed which aim to reduce the impact of design irregularities in P-wave surveys (Canning and Gardner, 1998; Jousset et al., 2000).

3D-PS Survey Design

3D PS-wave survey design has received literature attention over the past 15 years (e.g. Vermeer, 1999; Musser, 2005; Meier, 2009; Zuleta and Lawton, 2011). PS survey design is intrinsically more complex than P-wave design. Firstly the asymmetric nature of PS reflections leads to more irregular illumination.

In the context of PS data processing, the precise location of the asymmetric reflection point is very important for trace binning. Originally, PS processing included simplistic asymptotic binning (e.g. Eaton and Lawton, 1992) or various depth-dependent approaches (e.g. Tessmer and Behle, 1988; Zhang and Robinson, 1992; Schneider Jr, 2002). Specialized algorithms have been developed for converted-wave binning in situations where geology is more complicated (e.g. anisotropy (Thompson, 1999), dipping reflectors (Guarín, 2005)). Unfortunately, the most precise binning approaches require velocity information which is often unknown at the design stage.

As for P waves, specific PS-wave algorithms have been introduced which attempt to

minimize acquisition footprint arising during prestack migration (Lee et al., 2005; Vinje et al., 2015; Wang and Wang, 2014). Despite the availability of such tools, it is nevertheless desirable that PS surveys be designed with the aim of regular fold, offset and azimuth.

An additional difficulty in PS design is that the range of offsets that are usable for PS reflection may be restricted due to critical angle considerations (Garotta, 1999). Also, PS surveys are typically performed as an economical extension to a primary P-wave survey. Therefore a further restriction in PS survey design is that there should be minimal degradation in the associated P-wave data (Thomas and Neff, 2004).

Most previous analyses of PS survey design have focused mainly on conventional petroleum-scale exploration. In the following we examine aspects of PS design which are more specific to surveys at the coal scale.

OFFSET CONSIDERATIONS FOR COAL-SCALE PS DESIGN

In conventional P-wave seismic reflection a common rule of thumb is that maximum receiver offset should be comparable to target depth (e.g. Stone, 1994). This avoids possible phase distortions associated with post-critical reflections. For PS reflection, ray-path asymmetry implies that ideally maximum offset needs to be even less than for P waves if such distortions are to be avoided (Garotta, 1999).

One of the well-known problems of shallow seismic reflection is that noise events (e.g. surface waves, refractions) can often arrive in a similar time window to the target reflection events (e.g. Knapp and Steeples, 1986). It is typically necessary to increase minimum offset to avoid such high-amplitude surface-related noise (Hunter et al., 1984). The temptation is to incorporate longer offsets than might be considered acceptable according to normal rules of thumb. The viability of this approach can be examined via modeling exercises.

Figures 1 and 2 examine reflection behavior at the top and bottom of a typical coal seam. Consider first the P-wave reflection. Because the top of coal is an impedance decrease, the P-wave reflection has strong amplitude and constant phase over a wide range of incidence angles (Figure 1, red curve). At the base of coal (Figure 2, red curve) the P-wave amplitude is strong, and the phase is constant, for angles less than the critical angle. Of course, for incident angles greater than the critical angle, the phase behavior can change significantly. Based on this analysis, stacking of post-critical events would seem to be inadvisable.

Consider now the PS reflection (green curves in Figures 1 and 2). Amplitudes are low at small angles, suggesting that larger incidence angles (longer offsets) may be required to achieve a reasonable signal-to-noise ratio. For example, the green curves on Figures 1 and 2 show that the strongest PS reflections from the top and base of coal occur for angles $> 20°$. However, as was observed with the P-wave reflection, the phase angle varies significantly for the base-coal reflection in this zone. Again, inclusion of longer offsets would appear to be problematic.

The obvious approach to avoiding such phase problems is to follow the approach taken in petroleum-scale work, and limit the far offset such that the critical angle is not exceeded. This may, however, be difficult in practice. Consider a simple single-layer coal-seam model with parameters similar to those expected in our field trial (Table 1). Using ray-path modeling we have investigated the maximum allowable offset for seams of various thicknesses

(Figure 3). For this model, the maximum usable offset for PS reflection is approximately two-thirds that of P-wave reflection. This is consistent with the observations of Garotta (1999). For a 5m seam (corresponding to the expected thickness at the trial site) the maximum offsets would be 270m and 185m for P and PS reflections respectively. Based on expected weathering in the survey area, offsets less than about 50m are likely to be unusable. Hence on this analysis, the usable offset range is quite limited, particularly for the PS survey.

The ray-path modeling approach above provides a reasonable first indication of likely phase/offset limits. However, in practice, meaningful analysis of coal-seam response requires more detailed consideration of the full package of events from the seam. This has been demonstrated by Simmons Jr and Backus (1994), who used reflectivity modeling to determine the character of the total reflection package for a thin coal seam. Their work focused primarily on the zone within the critical angle.

In order to better understand the severity of phase distortion in our expected seam package, we have used visco-elastic finite-difference modeling to build synthetic seismic records (e.g. Robertsson et al., 1994). This wave-equation method incorporates P and S wave properties in the model, providing for mode conversions, surface waves, and also anelastic attenuation.

Figure 4 shows vertical and inline synthetic records corresponding to the geological model of Table 1, with a coal seam of thickness 5 m. The P-wave reflections are dominant on the vertical component. The energy of the reflection package is relatively consistent for all offsets. The red box indicates the P-wave offsets where the bottom-of-coal phase effects are expected. Close examination indicates that the character of the wavelet within the box is very similar to that of nearer offsets. This finite-difference analysis suggests that in practice the base-coal distortion has less influence on the seam package than predicted by simpler reflectivity modeling. This is consistent with field observations over a range of coal surveys.

As expected, the PS reflections are dominant on the inline component. The amplitude of the PS reflection increases with offset, having a significant portion of its energy beyond the critical angle (inside the green box). It is apparent that the post-critical reflections have a lagged response compared to the pre-critical offsets. Stacking all offsets together would result in a reduction in resolution of the final PS image. However, within the post-critical window the character is remarkably consistent. This suggests that post-critical reflections may be able to be stacked with each other without losing too much resolution, and maintaining a good signal-to-noise ratio.

These modeling results tend to be supported by our real-data observations, both from previous 2D-PS surveys, and from the 3D-PS trial. Figure 5a shows a representative common-conversion-point supergather from the 3D-PS trial. It includes a strong PS event corresponding to our target coal seam at depth 100m. On the near offsets (< 150m) this event has been swamped by noise. Most of the usable PS energy occurs at offsets beyond the predicted base-of-coal critical angle, consistent with modeling. While the data are generally noisy, the PS event tends to have reasonably consistent character over a range of offsets.

Figure 5b shows that it is possible to achieve a reasonably flat PS event over a range of offsets ($\sim 220 - 350$m), using a standard non-hyperbolic PS-NMO correction (e.g. Zhang, 1996). Note that further subtle resolution improvement can be obtained by using more

advanced PS-NMO algorithms (e.g. Strong and Hearn, 2012). These field observations add weight to the modeling results, and sugggest that PS events at offsets greater than the bottom-of-coal critical angle may be usable, provided the offset range is carefully chosen so as to maintain reasonably consistent character in the seam reflection package.

This fortuitous outcome is a result of the special physical properties of coal seams (low density and low velocity). We have reached similar conclusions when investigating relatively thin-seam scenarios in other locations. The general practical conclusion is that for typical coal exploration projects, the usable offset windows may be more generous than for petroleum-scale work. However, rigorous modeling is advised at the planning stage, as well as careful quality control during data processing.

ASYMMETRY CONSIDERATIONS FOR COAL-SCALE PS DESIGN

The analysis in the preceding section suggests that due to the particular characteristics of the target, the maximum usable offset for coal surveys may be greater (in relative terms) than for conventional reflection surveys. In particular, for PS surveys, modeling of the type illustrated above indicates that it may be possible to use offsets of order three times target depth. This in turn has implications for expected illumination patterns.

The asymmetry of PS waves has been heavily studied for several decades (e.g. Tessmer and Behle, 1988; Zhang and Robinson, 1992; Eaton and Lawton, 1992). For a simple horizontal reflector, the horizontal distance (X_P) from the source to the PS reflection point can be related to the source-detector offset (X_O) via

$$X_P = \frac{X_o}{1 + \tan\theta_S / \tan\theta_P} \tag{1}$$

where θ_P is the incident angle of the of the P-wave and θ_S is the reflection angle of the S-wave. These angles are related via Snell's law, and incorporate the depth and velocity dependence of the reflection point. The ray path is more asymmetric for shallower reflectors, and for larger values of the V_P to V_S ratio (γ).

To compare the degree of asymmetry expected in surveys at different scales (petroleum, coal), it is convenient to re-express the exact equation 1 as a relationship between the relative depth ($R = Z/X_o$) and relative offset ($C = X_P/X_o$) of the reflection point. (See Appendix A for details.)

$$R = \sqrt{\frac{(\gamma^2 - 1)C^2(1 - C)^2}{C^2 - \gamma^2(1 - C)^2}} \tag{2}$$

Figure 6 shows the relationship between relative depth (R) and relative offset (C), for various values of the velocity ratio (γ). Based on conventional rules of thumb, many petroleum surveys would fall in the zone beneath the R=1 line. On the other hand, coal-scale surveys are more likely to incorporate smaller values of R. As discussed above, offsets of up to three times target depth may sometimes be utilized, implying R values as low as 0.3. Figure 6 indicates that such surveys are more likely to utilize highly asymmetric rays. In addition it is more likely that the velocity ratio (γ) is more variable for shallower targets.

Figure 6 illustrates that this is likely to introduce further variability and complexity into PS ray-paths.

In Figure 6 the depth zone deeper than R=1 represents the area for which the horizontal reflection point is relatively constant. In this zone, the so-called asymptotic approximation (e.g. Eaton and Lawton, 1992; Hardage et al., 2011) might provide a usable estimate of reflection point for the purposes of survey design. This might be acceptable for petroleum-scale surveys if very limited velocity information is available at the time of design. However, the preceding analysis suggests that for coal-scale surveys incorporating longer relative offsets, the design must be carried out using more precise depth-dependent reflection-point estimators (e.g. Tessmer and Behle, 1988; Zhang and Robinson, 1992; Hoffmann, 2001). If limited velocity information is available, the implications of likely velocity ranges should be considered during the design process.

3D-PS SURVEY-DESIGN CASE STUDY

Overview of design methodology

One of the primary aims of our real data experiment was to explore possible azimuthal anisotropy in both P-wave and S-wave velocities, as an aid to better understanding the stress regime in the study area. Such information would be important at the mine-planning stage, for economic and safety reasons. It was therefore desirable to achieve a reasonably smooth distributions of fold, offset and azimuth in both the P and PS designs.

The initial 3D-PS design process assumed a nominal target depth of 100m, based on a previous 2D P-wave survey. The effective velocity-ratio (γ) to the target is unknown, although 2D-3C experience in the region suggested a likely range of values. In practice, the design needed to be acceptable over the full extent of possible γ values. A PS survey such as this would generally be considered as an extension to a production P-wave 3D survey. Hence, the design parameters needed to be broadly consistent with typical 3D P-wave surveys over similar targets.

In the results to follow the exact conversion point has been calculated (using equation 2) based on an assumed target depth and velocity ratio. If perfect specular reflection is assumed, the predicted patterns of fold, offset and azimuth exhibit a larger degree of variability, and sensitivity, than might be expected with real data (e.g. Eaton and Lawton, 1992). The finite bandwidth of a real seismic wave can be incorporated into the design process by recognizing that each individual trace may contribute (in terms of fold, offset, azimuth) to multiple bins. This more accurately resembles the situation after migration-based processing. We follow the approach of Cary and Lawton (2003) who smear the trace using a sinc smoothing function. The examples to follow use a related Lanczos filter, which in some cases may provide a more stable output (Ye and Entezari, 2012). Again following Cary and Lawton (2003), we set the radius of the smoothing filter to the bin size. This implicitly assumes that the chosen bin size is appropriate to the expected horizontal resolution following migration.

In the present case, this approach appears reasonable based on the resolution following 3D prestack migration, as suggested by Chen and Schuster (1999). We have related the radius of our smoothing filter to Chen and Schuster's sinc-function radius ($x_i = \Delta x/2$). If

we assume a usable migration aperture of twice target depth, and dominant frequency of order 100 Hz, a smoothing radius of 10-15m appears reasonable. This then provides a guide for choosing bin sizes.

General design conclusions

The series of design examples to follow step through a range of possible geometries, starting with theoretically ideal high-density designs and moving towards more practically feasible designs, including the final real-survey design. The starting scenario is a simple orthogonal geometry, with sources on a 15m x 15m grid, and receivers also on a 15m x 15m grid. We start with an assumed bin size of 7.5m x 7.5m, which might be considered natural for a P-wave survey.

Figure 7 summarizes relative fold, offset and azimuth distributions for P and PS surveys for this initial geometry. The figure layout (which is the same for subsequent plots) requires explanation. The left hand column shows fold distributions for a representative zone of 8 x 8 bins. From top to bottom, the plots are for P-wave, PS-wave ($\gamma = 2$), PS-wave ($\gamma = 3$). The two PS plots are provided to illustrate how the distribution behaves over the most likely range of γ values. (As part of our full work-flow we have also monitored other γ values.) Alongside each fold plot are the offset-azimuth distributions for the central 4 bins (marked in white on the fold plot). Four bins are included to illustrate bin-to-bin variability in these parameters. In the offset-azimuth plots, the maximum inline and crossline offsets are 300m in all cases.

Figure 7 shows that, with this high-density design, the fold is very consistent for both P and PS surveys. The offset-azimuth distribution is regular for P, but is much more variable for PS. Figure 8 illustrates that the offset-azimuth distribution improves dramatically if the bin size is doubled, so that it matches the source and receiver grid size (15m). This could then be considered as a theoretically ideal orthogonal grid for PS, with very regular distributions of fold and offset-azimuth. In most practical cases, we will need to examine more cost effective geometries. We will first examine reductions in either receiver density or source density. To emphasize the effect we will make significant reductions in density.

In cases where Vibroseis is planned, a natural approach might be to reduce the receiver density, while maintaining higher source density. Figure 9 considers the case where the receiver grid is changed from 15m x 15m to 60m x 60m. Source density is left high at 15m x 15m. The P-wave design (top row) shows a very regular fold, and an even distribution of offset-azimuth. However, the PS results are much less acceptable, with relative fold and offset-azimuth being very irregular. In addition, the PS distributions appear very sensitive to the assumed value of γ.

Figure 10 illustrates the opposite approach where the receiver density is kept high at 15m x 15m, and the source grid is changed to 60m x 60m. Again, for P waves, relative fold is constant, and offset-azimuth shows a regular distribution. With this approach the PS results are much more acceptable. Fold is acceptably smooth, and the offset-azimuth distribution is much improved compared to Figure 9. PS designs with reduced source effort would be particularly attractive in cases where a dynamite source is considered. This is an important observation for 3D coal surveys, where high resolution is very valuable for mine-planning purposes.

Final 3D-PS survey design

Unfortunately, a 15m x 15m receiver grid would not be economic for most coal-scale surveys. To achieve a final practical design, a variety of combinations were examined, with consideration of logistical and economic constraints. Figure 11 shows results for an orthogonal design with densities similar to the final design (source grid: 30m x 30m, receiver grid: 15m x 30m, bins: 15m x 30m). Fold is regular for P and PS. While offset-azimuth distribution is not as smooth as for the higher-density designs, it is acceptable.

It has been suggested that orthogonal designs may introduce a cyclic acquisition footprint in fold images, and various methods have been proposed to reduce this problem. These include infield techniques such as staggered grids (e.g. Bland et al., 1998), brick patterns (e.g. Lawton, 1994), non-orthogonal geometries (e.g. Cordsen et al., 2000), and random jitter (Hardage et al., 2011); and post-acquisition processing techniques that interpolate even bin distributions (e.g. flexi bin, Lawton et al., 1995). For this investigation, we have focused on the non-orthogonal method since this is easier to implement in the field and has proven successful for P-wave coal-scale exploration.

The final design incorporated source and receiver densities similar to those in Figure 11, but with source lines at 60° to the receiver lines. Figure 12 provides a graphical representation of the basic survey geometry and its caption includes details of relevant survey statistics.

The corresponding fold and offset-azimuth predictions are given in Figure 13. Compared to the orthogonal grid (Figure 11), the P-wave offset-azimuths are arguably slightly more randomized. The PS offset-azimuth distribution appears slightly less variable (i.e. more stable color distribution).

The design analyses given to this point have been for a nominal target depth of 100m. A previous 2D P-wave line suggested that the actual target depth in the area of the planned 3D varied from about 85m to 140m (Figure 14). The preferred design was confirmed for a range of target depths across the survey area. For example, Figure 15 shows the predicted distributions in the area where the target is deepest (140m). As expected (based on equation 2), the offset-azimuth points are shifted compared to the 100m analysis in Figure 13. However, the overall distribution is of similar quality. This is also the case for other target depths examined.

CONCLUSION

Survey design for 3D-PS reflection is more complicated than for P-wave reflection, with ray-path asymmetry dependent on target depth and velocities. These problems may be more apparent at the coal-scale (target depth 0-300m) than at the conventional petroleum scale.

Coal-scale PS records typically suffer strong noise interference at short offsets. Simple ray-path analysis for typical seams suggests that post-critical reflections from the base-of-coal might seriously restrict usable far offsets. The conventional approach of excluding all post-critical arrivals would result in poor fold in the case of PS data. A useful tool for assessing the severity of such phase distortion is finite-difference modeling. For typical seam parameters, this modeling suggests that the post-critical zone may in some cases be usable.

The P-wave reflection package often exhibits relatively consistent phase across the offset range. The character of PS reflections can also be quite consistent within the post-critical zone, where amplitudes are also high.

The incorporation of such longer-offset data requires careful selection of offset ranges, and rigorous quality control in processing. However, it is often possible to significantly increase the signal-to-noise ratio, with only minimal degradation in resolution. Depending on survey objectives, this may be a worthwhile compromise. The tendency to include longer offsets has a serious implication for coal-scale PS survey design, in that it is more likely to incorporate rays which are highly asymmetrical, and very sensitive to choice of the V_P/V_S velocity ratio.

A case study of a coal-scale 3D-PS survey design has been presented. A general observation, consistent with previous petroleum-scale studies, is that for the P-wave design, reducing source or receiver density has a similar impact on fold and offset-azimuth distributions. However in the case of the PS design, reduction in source density is the preferred option. This is an important observation in the coal seismology context, where dynamite surveys are relatively common, with the aim of maximizing resolution for mine planning.

The final preferred design incorporated a slanted source line geometry. These adjustments appear to have marginally reduced the variations in PS offset-azimuths, compared with the related orthogonal design. The offset-azimuth distribution of the P-wave data has changed but in this case the overall impact on the P-wave processing is likely to be negligible.

Any seismic survey design must include logistic, economic, and environmental factors. These sometimes compete against the resolution requirements. For the specific 3D-3C trial considered here, a reasonable balance of these was achieved. The overall results of the trial are presented elsewhere (Strong and Hearn, 2011). The offset-azimuth distribution achieved across the survey has permitted the detection of clear azimuthal anisotropy in both P and PS data, with convincing relationships to fault structures and associated stress directions (Hearn and Strong, 2012). The success of that analysis was dependent on careful P and PS survey design.

While this investigation has focused on the coal-scale, the concepts are also relevant to more conventional surveys where knowledge of the near surface may be important for velocity and anisotropy analysis.

ACKNOWLEDGMENTS

We would like to acknowledge the Australian Coal Association Research Program (ACARP) for their support of this research, and the host mine site for access to the test site. We thank Associate Editor Guy Drijkoningen, and reviewers Denis Mougenot, Peter Cary, and two anonymous, whose suggestions greatly improved the paper.

REFERENCES

Barkved, O. I., M. C. Mueller, and L. Thomsen, 1999, Vector interpretation of the Valhall 3D/4C OBS dataset: 61st Mtg., Eur. Assn. Geosci. Eng., Session:6042.

Bland, H. C., R. R. Stewart, H.-x. Lu, A. Cordsen, and M. Werner, 1998, The shaganappi geotechnical experiments: 2-D and 3-D multicomponent seismic surveys and geologic logs: Technical Report 34, CREWES Research Report.

Canning, A., and G. H. Gardner, 1998, Reducing 3-D acquisition footprint for 3-D DMO and 3-D prestack migration: Geophysics, **63**, 1177–1183.

Cary, P. W., 1999, Common-offset-vector gathers: an alternative to cross-spreads for wide-azimuth 3-D surveys: Presented at the 1999 SEG Annual Meeting, Society of Exploration Geophysicists.

Cary, P. W., and D. C. Lawton, 2003, Bandlimited design and stacking of PP and PS surveys: Presented at the 2003 SEG Annual Meeting, Society of Exploration Geophysicists.

Chemingui, N., and B. Biondi, 1996, Handling the irregular geometry in wide-azimuth survays: 1996 SEG Annual Meeting, Society of Exploration Geophysicist, 32–35.

Chen, J., and G. T. Schuster, 1999, Resolution limits of migrated images: Geophysics, **64**, 1046–1053.

Cooper, N., 2004, Tutorial A world of reality Designing land 3D programs for signal, noise, and prestack migration; Part 1: The Leading Edge, **23**, 1007–1014.

Cordsen, A., M. Galbraith, and J. Peirce, 2000, *in* Planning Land 3-D Seismic Surveys: Society of Exploration Geophysicists, Geophysical Development, No. 9, 204.

Crewes.org, 2005, CREWES Zoeppritz Explorer 2.2.

Dufour, J., J. Squires, W. N. Goodway, A. Edmunds, and I. Shook, 2002, Integrated geological and geophysical interpretation case study, and lamé rock parameter extractions using AVO analysis on the blackfoot 3C-3D seismic data, southern Alberta, Canada: Geophysics, **67**, 27–37.

Eaton, D. W., and D. C. Lawton, 1992, P-SV stacking charts and binning periodicity: Geophysics, **57**, 745–748.

Gardner, G. H., and A. Canning, 1994, Effects of irregular sampling on 3D prestack migration: 1994 SEG Annual Meeting, Society of Exploration Geophysicist, 1553–1556.

Garotta, R., 1999, Shear waves from acquisition to interpretation: 2000 distinguished instructor short course: Society of Exploration Geophysicists.

Guarín, A. T., 2005, On the calculation of P-SV conversion point for a dipping bed: Geophysics, **71**, T13–T16.

Hanson, R. A., M. K. MacLeod, C. R. Bell, C. J. Thompson, and J. Somod, 1999, Multicomponent seismic interpretation - data integration issues, Alba field, North Sea: 61st Mtg., Eur. Assn. Geosci. Eng., Session:6027.

Hardage, B. A., M. V. DeAngelo, P. E. Murray, and D. Sava, 2011, *in* Multicomponent seismic technology: Society of Exploration Geophysicists, Geophysical Reference Series, No. 18, 318.

Hearn, S., and S. Strong, 2012, Investigation of azimuthal anisotropy in high-fold 3D multicomponent seismic reflection: ASEG Extended Abstracts, **2012**, 1–4.

Hearn, S. J., 2004, Shallow, high-resolution converted-wave seismology for coal exploration: Presented at the 17th meeting, Sydney, Aust. Soc. Expl. Geoph.

Hendrick, N., 2006, Converted-wave seismology for coal exploration: Recorder: Canadian Society of Exploration Geophysicists May, 27, **31**.

Hoffmann, J., 2001, Illumination, resolution, and image quality of PP- and PS-waves for survey planning: The leading edge, **20**, 1008–1014.

Hunter, J., S. Pullan, R. Burns, R. Gagne, and R. Good, 1984, Shallow seismic reflection mapping of the overburden-bedrock interface with the engineering seismograph-some simple techniques: Geophysics, **49**, 1381–1385.

Jousset, P., P. Thierry, and G. Lambaré, 2000, Improvement of 3D migration/inversion by reducing acquisition footprints: Application to real data: Presented at the 2000 SEG Annual Meeting, Society of Exploration Geophysicists.

Knapp, R. W., and D. W. Steeples, 1986, High-resolution common-depth-point reflection profiling: Field acquisition parameter design: Geophysics, **51**, 283–294.

Lawton, D. C., 1994, Acquisition design for 3-D converted waves: Technical Report 23, CREWES Research Report.

Lawton, D. C., R. R. Stewart, A. Cordsen, and S. Hrycak, 1995, Advances in 3C-3D design for converted waves: Technical Report 7(43), CREWES Research Report.

Lee, S.-S., J. Willis, and S. Lin, 2005, Migration weights for pre-stack converted wave data to reduce the acquisition footprint: Presented at the 2005 SEG Annual Meeting, Society of Exploration Geophysicists.

Liner, C. L., and W. D. Underwood, 1999, 3-D seismic survey design for linear v(z) media: Geophysics, **64**, 486–493.

Meier, M. A., 2009, Converted-wave survey design: Presented at the 2009 SEG Annual Meeting, Society of Exploration Geophysicists.

Musser, J. A., 2005, Full-Wave 3D Seismic Survey Designs and Operations for the Marine Environment: Presented at the 2005 SEG Annual Meeting, Society of Exploration Geophysicists.

Robertsson, J. O., J. O. Blanch, and W. W. Symes, 1994, Viscoelastic finite-difference modeling: Geophysics, **59**, 1444–1456.

Schneider Jr, W. A., 2002, A simple, exact solution for the P-SV wave conversion point via prestack migration: Geophysics, **67**, 1634–1636.

Simmons Jr, J. L., and M. M. Backus, 1994, AVO modeling and the locally converted shear wave: Geophysics, **59**, 1237–1248.

Stone, D., 1994, Designing seismic surveys in two and three dimensions: Society of Exploration Geophysicists. Geophysical References Series, No. 5.

Strong, S., and S. Hearn, 2011, Towards 3D, integrated P+PS seismic imaging of coal targets: Technical report, Australian Coal Associaiton Research Program (ACARP) Report, C17029.

———, 2012, The importance of non-hyperbolic and stretch effects in far-offset P and PS nmo processing: ASEG Extended Abstracts, **2012**, 1–4.

Tessmer, G., and A. Behle, 1988, Common reflection point data-stacking technique for converted waves: Geophysical Prospecting, **36**, 671–688.

Thomas, J. W., and W. Neff, 2004, Teepee technology applied to C-wave acquisition design: The Leading Edge, **23**, 1049–1052.

Thompson, L., 1999, Converted-wave reflection seismology over inhomogeneous, anisotropic media: Geophysics, **23**, 678–690.

Vermeer, G. J., 1998, Creating image gathers in the absence of proper common-offset gathers: Exploration Geophysics, **29**, 636–642.

———, 1999, Converted waves: properties and 3D survey design: Presented at the 1999 SEG Annual Meeting, Society of Exploration Geophysicists.

Vinje, V., P. Zhao, and J. Gaiser, 2015, Offset vector tile gather extension and weighting to reduce footprint in dual-datum and converted-wave migration: Presented at the 2015 SEG Annual Meeting, Society of Exploration Geophysicists.

Wang, S., and J. Wang, 2014, 5D interpolation/regularization and COV/OVT PSTM for converted-wave (PS) data: SEG Technical Program Expanded Abstracts 2014, 3584–3588.

Ye, W., and A. Entezari, 2012, A geometric construction of multivariate sinc functions: Image Processing, IEEE Transactions on, **21**, 2969–2979.

Zhang, Y., 1996, Nonhyperbolic converted wave velocity analysis and normal moveout: Presented at the 1996 SEG Annual Meeting, Society of Exploration Geophysicists.

Zhang, Y., and E. A. Robinson, 1992, Stacking P-SV converted wave data with raypath velocity: Presented at the 1992 SEG Annual Meeting, Society of Exploration Geophysicists.

Zuleta, L. M., and D. C. Lawton, 2011, PS survey design: Presented at the 2011 SEG Annual Meeting, Society of Exploration Geophysicists.

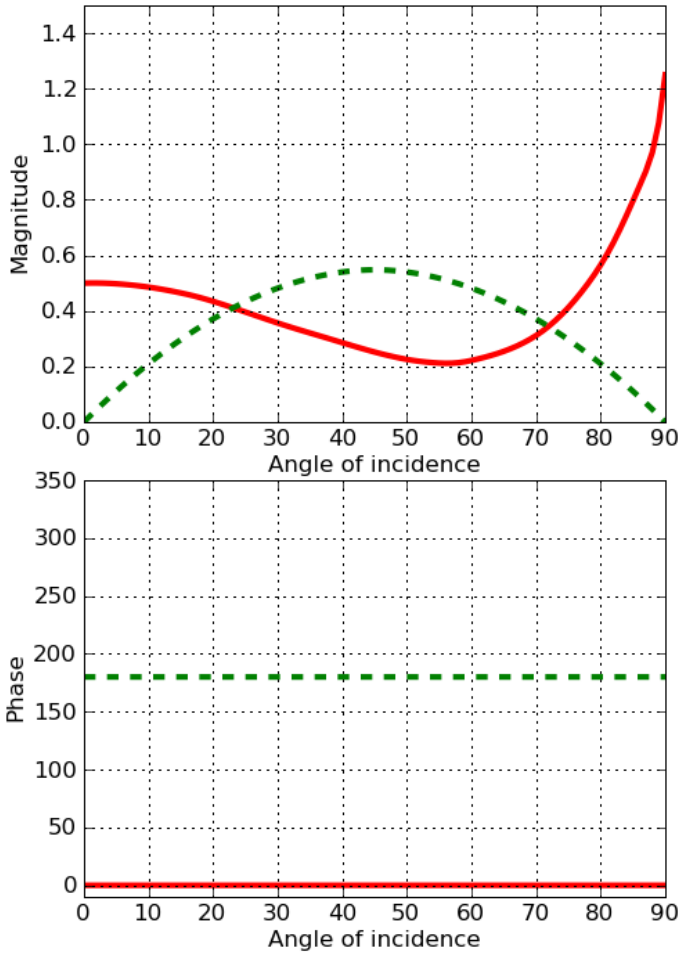

Figure 1: Top-of-coal response for P (red) and PS (green) reflections. Magnitude (top) and phase (bottom) variations are shown as a function of angle of incidence (and hence offset). Coal: V_P=2250 m/s; V_S=900 m/s; ρ=1400 kg/m^3. Sedimentary rock: V_P=3200 m/s; V_S=1600 m/s; ρ=2500 kg/m^3. The curves were generated using CREWES Zoeppritz Explorer 2.2 (Crewes.org, 2005).

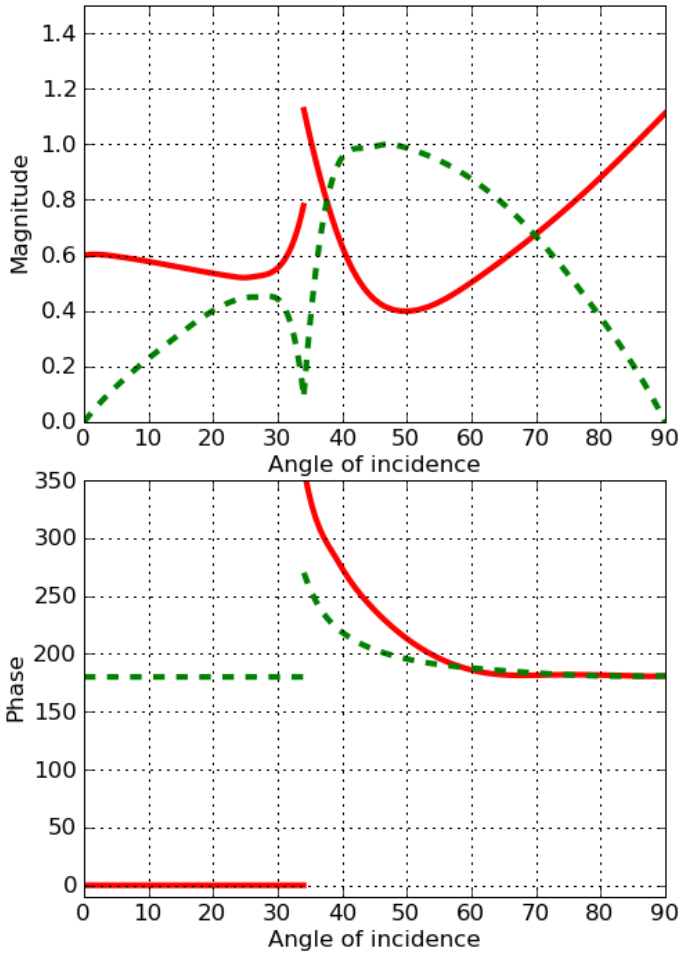

Figure 2: Bottom-of-coal response for P (red) and PS (green) reflections. Magnitude (top) and phase (bottom) variations are shown as a function of angle of incidence (and hence offset). Layer parameters as for Figure 1 . The curves were generated using CREWES Zoeppritz Explorer 2.2 (Crewes.org, 2005). Phase response for both wave types changes significantly at the critical angle (approximately 34°).

Layer	V_P **(m/s)**	V_S **(m/s)**	ρ **(kg/m^3)**	**Thickness (m)**
Country rock 1	3200	1600	2500	100
Coal	2250	900	1400	≥ 5
Country rock 2	4000	2000	2500	∞

Table 1: Coal seam model used in the phase vs. offset analysis. The parameters shown are indicative of those expected in the real field trial.

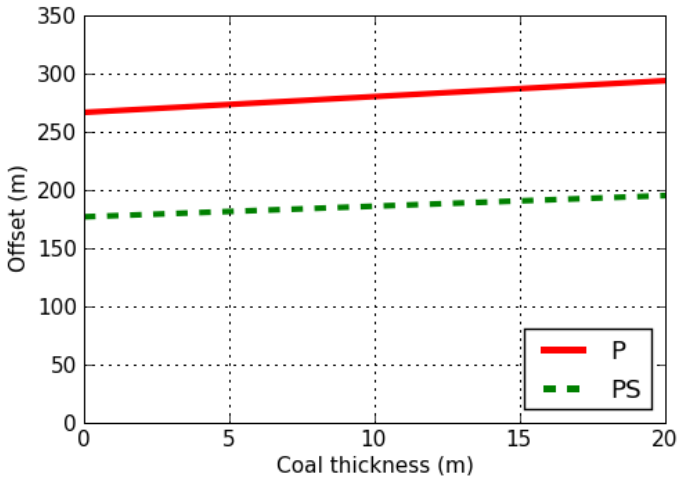

Figure 3: Ray-path modeling to estimate offset at which critical-angle phase distortion is expected, for coal seams of various thicknesses. Model parameters are given in Table 1. For a 5 m seam, P (red) and PS (green) distortion is predicted beyond 270m and 185m respectively.

APPENDIX A

RELATIONSHIP BETWEEN RELATIVE DEPTH AND RELATIVE OFFSET FOR A PS REFLECTION POINT

Repeating equation 1 for convenience, the PS reflection point offset is given by

$$X_P = \frac{X_o}{1 + \frac{\tan\theta_S}{\tan\theta_P}} \tag{A-1}$$

where X_o is the offset, θ_P is the incident angle of the downgoing P-wave and θ_S is the reflection angle of the upgoing S-wave. For comparative survey-design analyses, it is useful to re-express this equation as a relationship between the relative depth ($R = Z/X_o$) and relative offset ($C = X_P/X_o$) of the reflection point. Equation A-1 becomes

$$C = \frac{1}{1 + \frac{\tan\theta_S}{\tan\theta_P}} \tag{A-2}$$

or

$$C = \frac{1}{1 + \frac{\sin\theta_S \cos\theta_P}{\sin\theta_P \cos\theta_S}}. \tag{A-3}$$

We use Snell's Law

$$\gamma = \frac{V_P}{V_s} = \frac{\sin\theta_P}{\sin\theta_S} \tag{A-4}$$

and also introduce D_P and D_S corresponding to the distance traveled by the P and S waves respectively

$$\cos\theta_P = \frac{Z}{D_P},\ \cos\theta_S = \frac{Z}{D_S}. \tag{A-5}$$

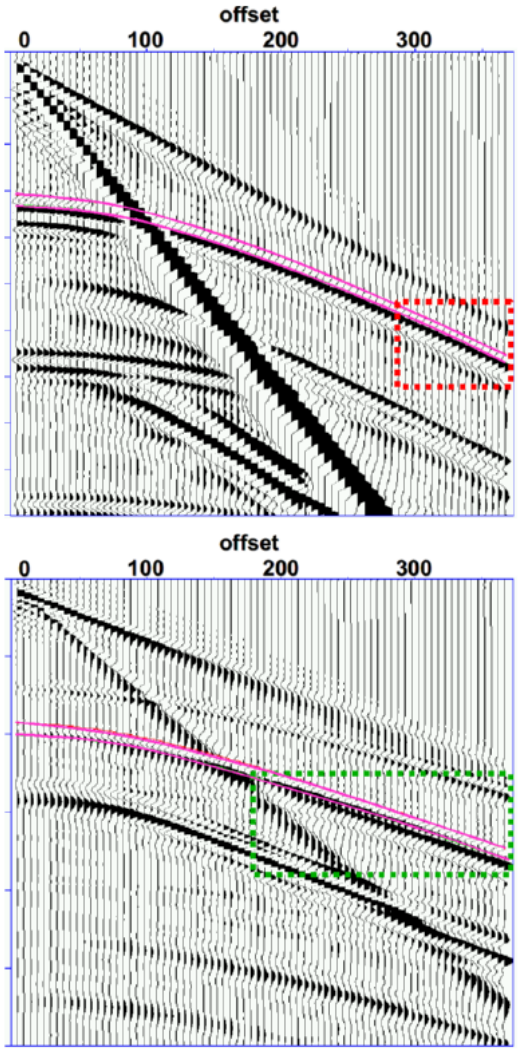

Figure 4: Finite-difference evaluation of phase vs offset distortion for the model in Table 1. On the vertical component record (top) post-critical P-wave distortion is much less pronounced (red box) than for the PS reflection on the inline horizontal record (bottom, green box). Reflection times for top and bottom of the seam are indicated by the magenta lines. A minimum-phase wavelet has been used in the modeling. To aid comparison, the vertical scale has been stretched on the vertical record. Total time scales are vertical (top): 0.2s, inline (bottom): 0.3s.

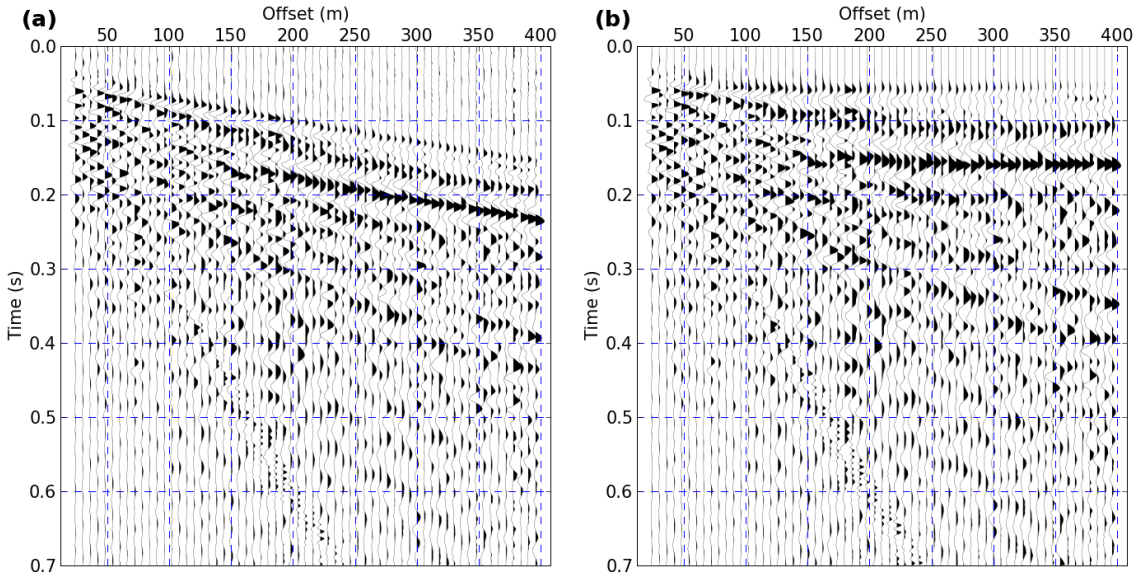

Figure 5: Inline common-conversion-point super gather from 3D-PS trial. (a) record showing a strong PS reflection event corresponding to target coal-seam. The modeling in Figure 3 suggests the base-of-coal critical angle corresponds to an offset of approximately 185 m. (b) record after non-hyperbolic PS-NMO, $V_P = 3200$m/s, V_P/V_S ratio (γ) = 2.4.

Hence equation A-3 becomes

$$C = \frac{1}{1 + \frac{D_S}{\gamma D_P}} \tag{A-6}$$

Rearranging and squaring gives

$$\frac{D_P^2}{D_S^2} = \frac{C^2}{\gamma^2(1-C)^2}. \tag{A-7}$$

Using Pythagoras' Theorem, we also have

$$\frac{D_P^2}{D_S^2} = \frac{X_P^2 + Z^2}{(X_O - X_P)^2 + Z^2} \tag{A-8}$$

or, in terms of the relative depth $R = \frac{Z}{X_O}$ and relative offset $C = \frac{X_P}{X_O}$

$$\frac{D_P^2}{D_S^2} = \frac{C^2 + R^2}{(1-C)^2 + R^2}. \tag{A-9}$$

Equating A-7 and A-9

$$\frac{C^2 + R^2}{(1-C)^2 + R^2} = \frac{C^2}{\gamma^2(1-C)^2}. \tag{A-10}$$

Rearranging gives

$$R^2 = \frac{(\gamma^2 - 1)C^2(1-C)^2}{C^2 - \gamma^2(1-C)^2} \tag{A-11}$$

or

$$R = \sqrt{\frac{(\gamma^2 - 1)C^2(1-C)^2}{C^2 - \gamma^2(1-C)^2}}. \tag{A-12}$$

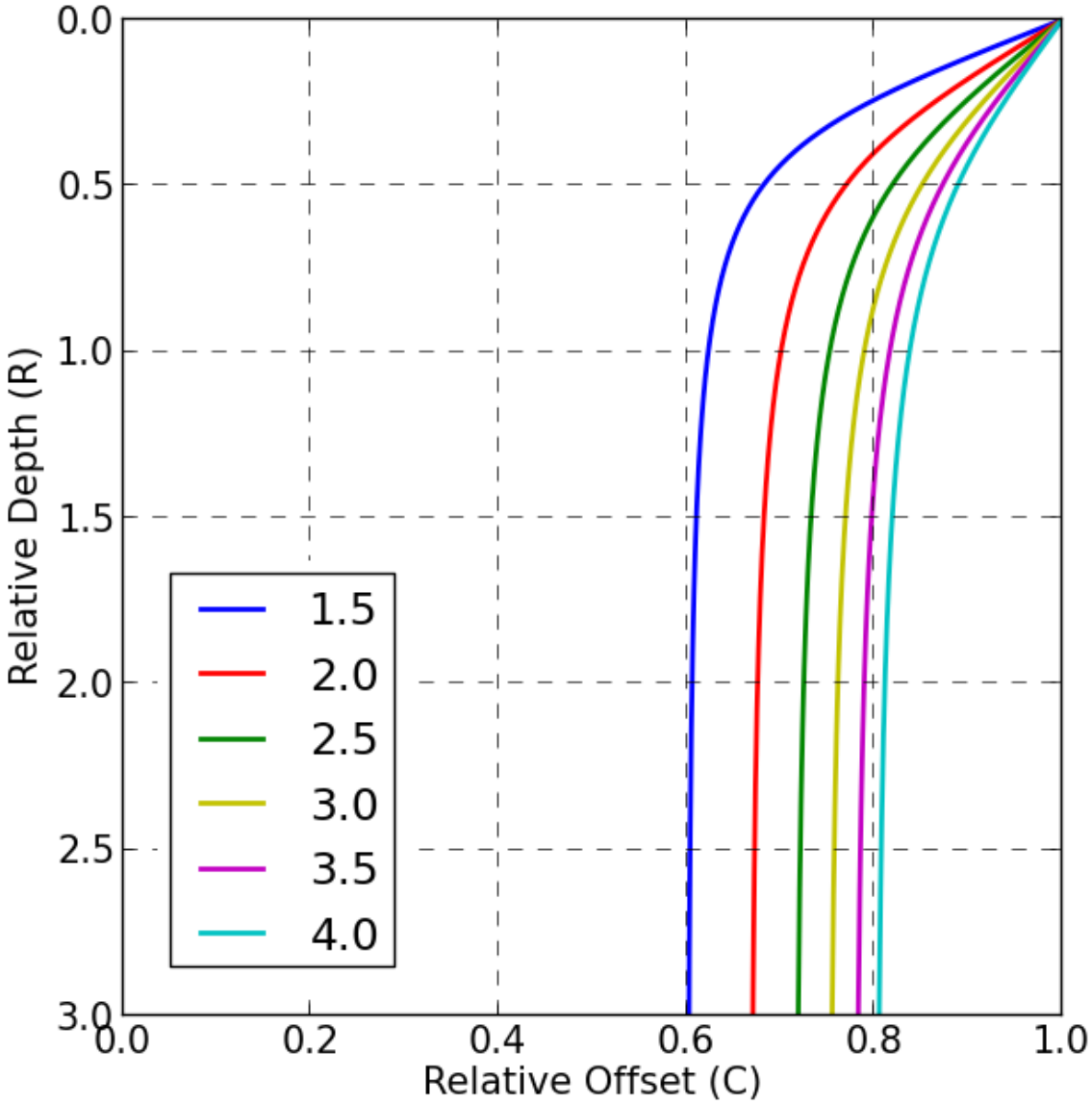

Figure 6: Relative depth (R) versus relative offset (C) of PS reflection point, for a typical range of γ values (different colors), as derived using equation 2. Coal-scale surveys are more likely to incorporate highly asymmetric rays in the zone above R=1.

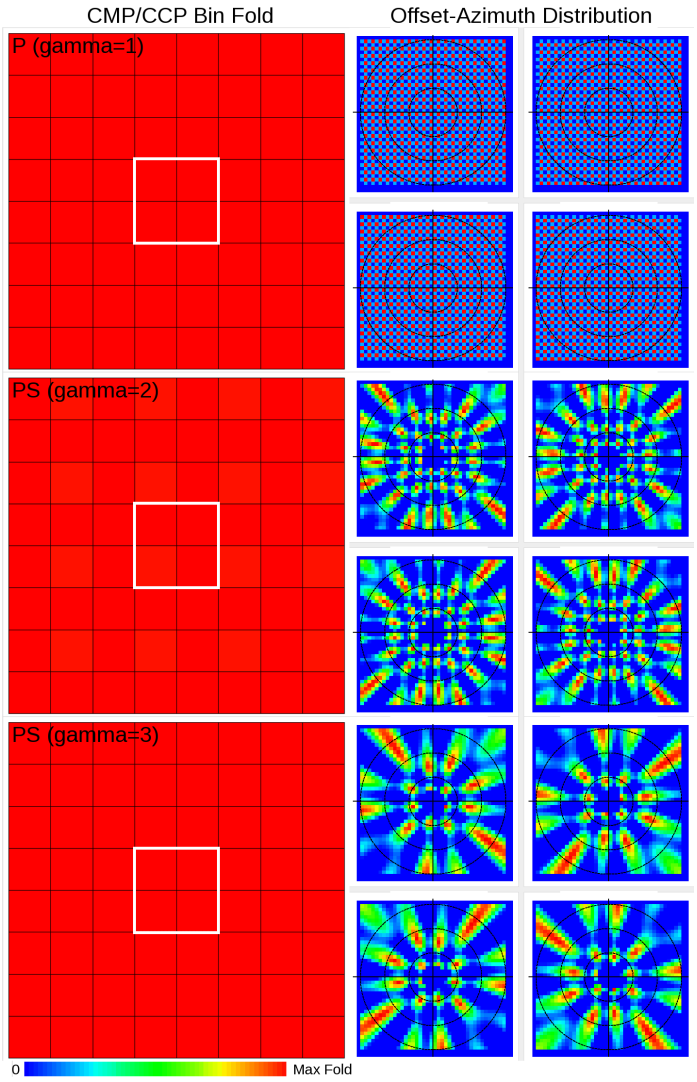

Figure 7: Comparison of bin fold (Left) and offset-azimuth distribution (Right) for P waves (top), and PS waves ($\gamma = 2$ mid, $\gamma = 3$ bottom). The offset-azimuth plots correspond to the four reflection bins marked by the white square. Each of these are gridded based on 15m x 15m common offset tiles. A Lanczos sinc filter has been applied to all reflections. This layout will be consistent for the following images. Geometry: Orthogonal grid, Source 15m x 15m, Receivers 15m x 15m, Bin 7.5m x 7.5m, Target depth 100m.

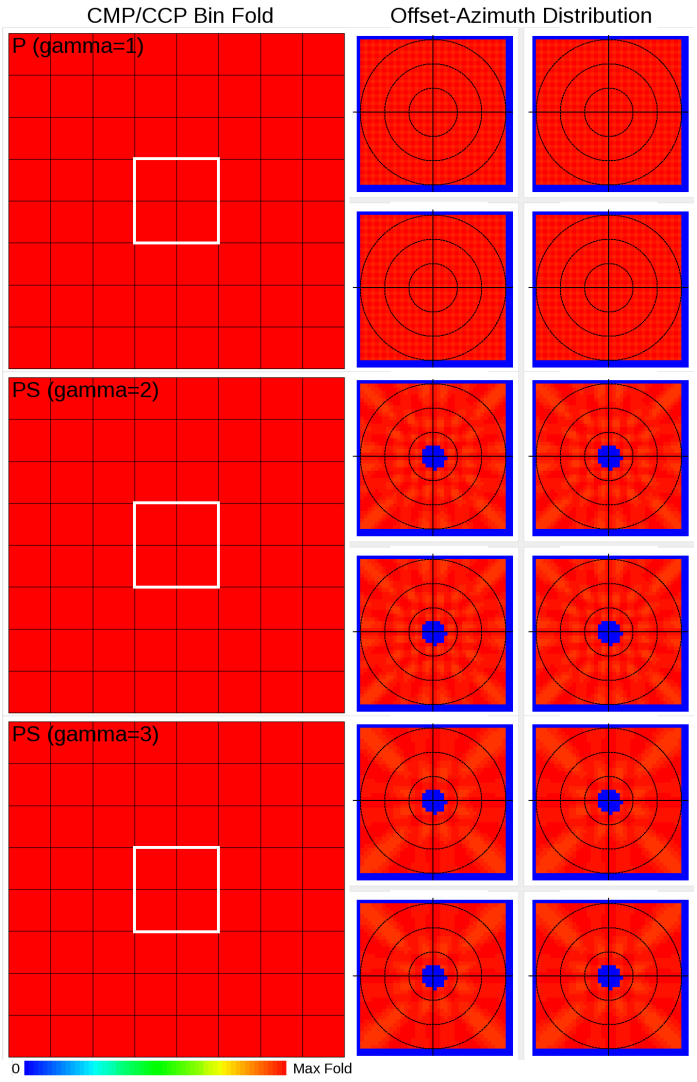

Figure 8: Fold, azimuth/offset distribution for larger bins compared to Figure 7. Geometry: Orthogonal grid, Source 15m x 15m, Receivers 15m x 15m, Bin 15m x 15m, Target depth 100m.

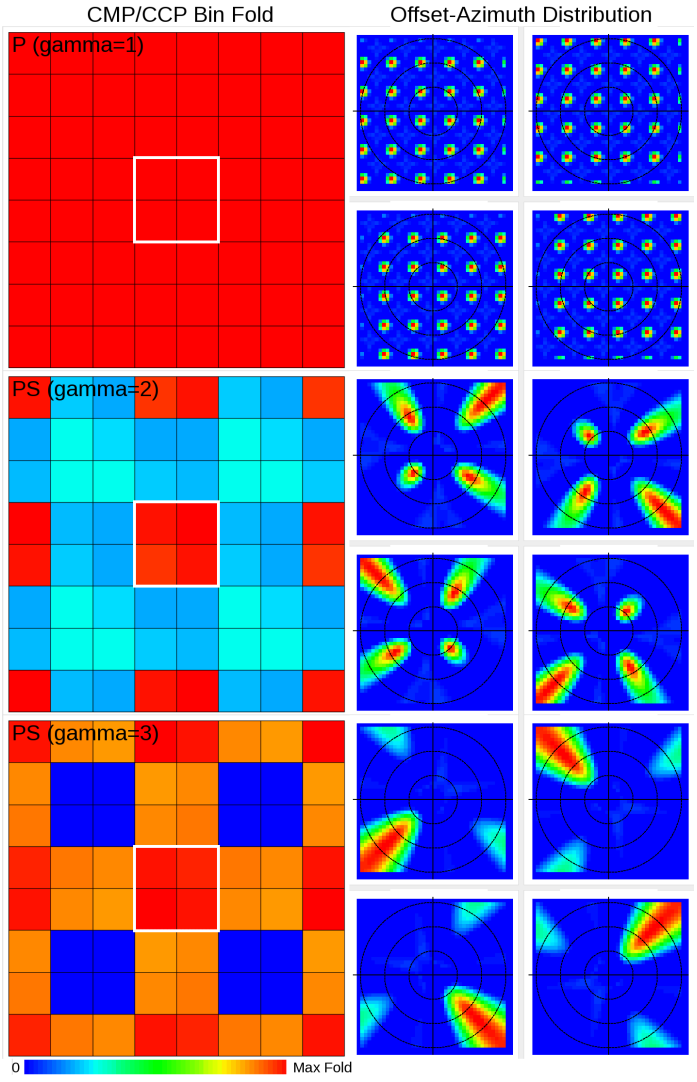

Figure 9: Decimation of receivers, compared to Figure 8 . Geometry: Orthogonal grid, Source 15m x 15m, Receivers 60m x 60m, Bin 15m x 15m, Target depth 100m.

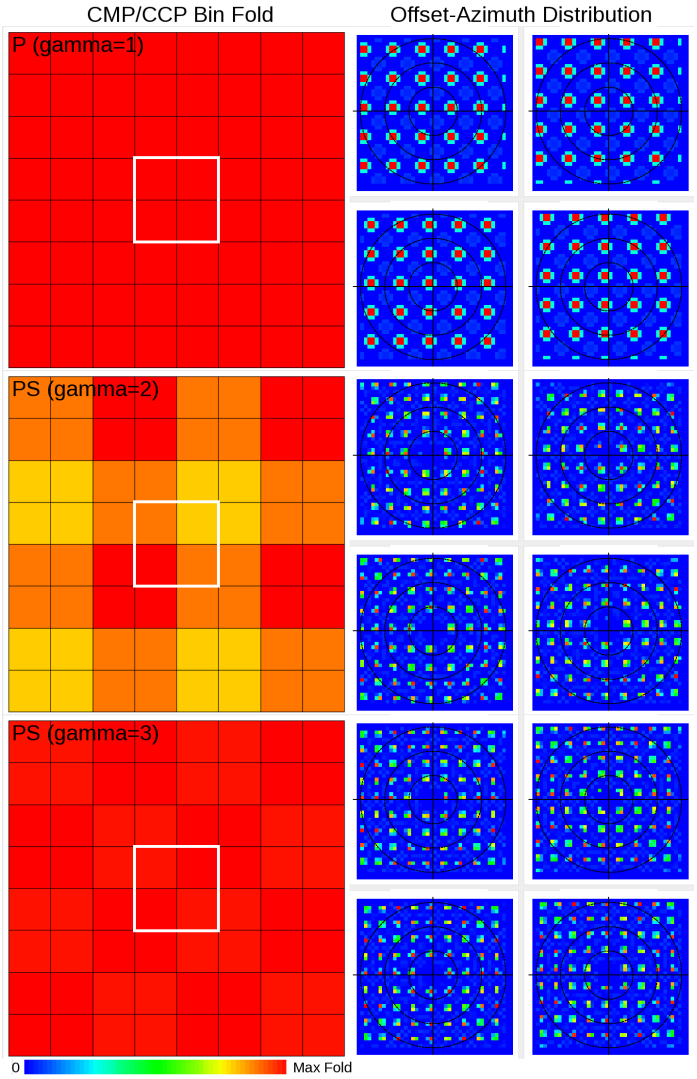

Figure 10: Decimation of sources for comparison to Figure 9. Geometry: Orthogonal grid, Source 60m x 60m, Receivers 15m x 15m, Bin 15m x 15m, Target depth 100m.

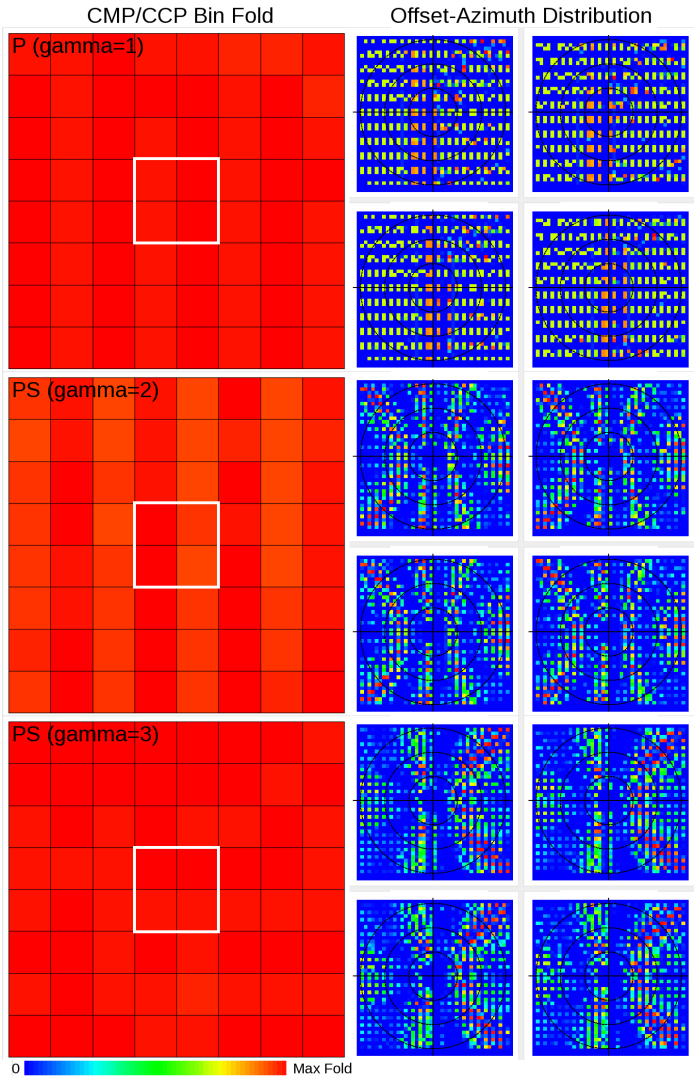

Figure 11: Reduction in source and receiver densities for economic purposes. Geometry: Orthogonal grid, Source 30m x 30m, Receivers 15m x 30m, Bin 15m x 30m, target depth 100m.

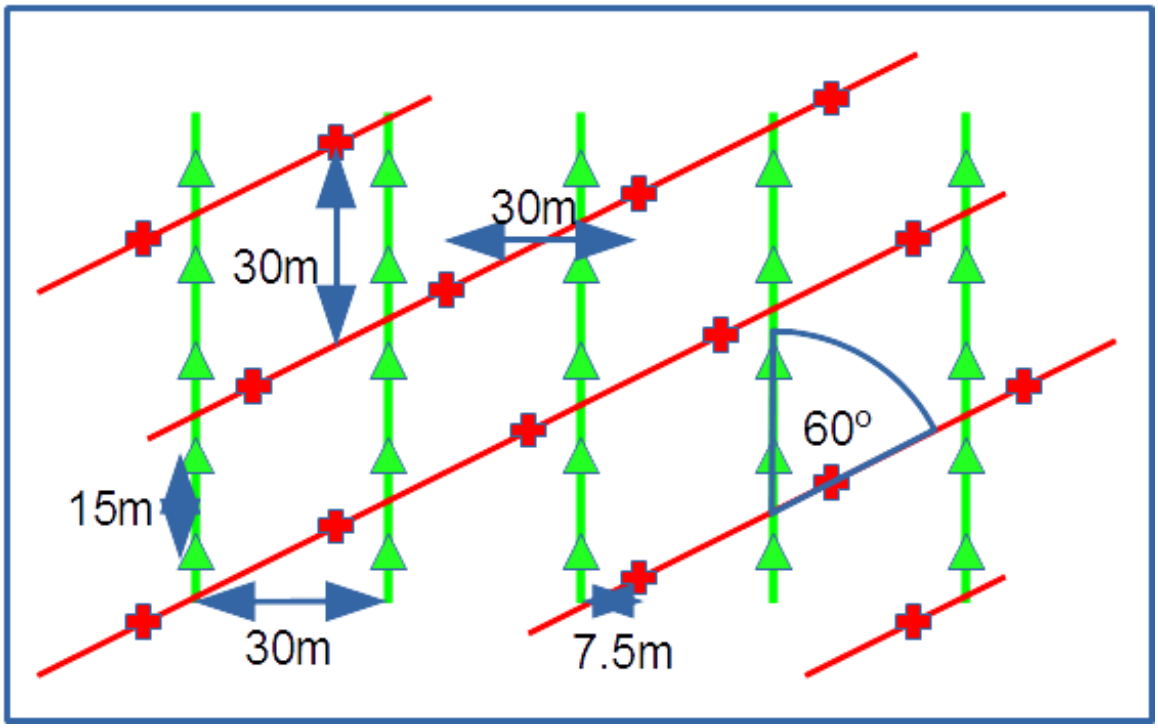

Figure 12: Sample of the final acquisition geometry: source lines (red), source locations (crosses), receiver lines (green) and receiver locations (triangles). The survey consisted of a fixed spread with 660 receiver locations across 10 lines, 594 source locations across 44 lines at a 60° orientation.

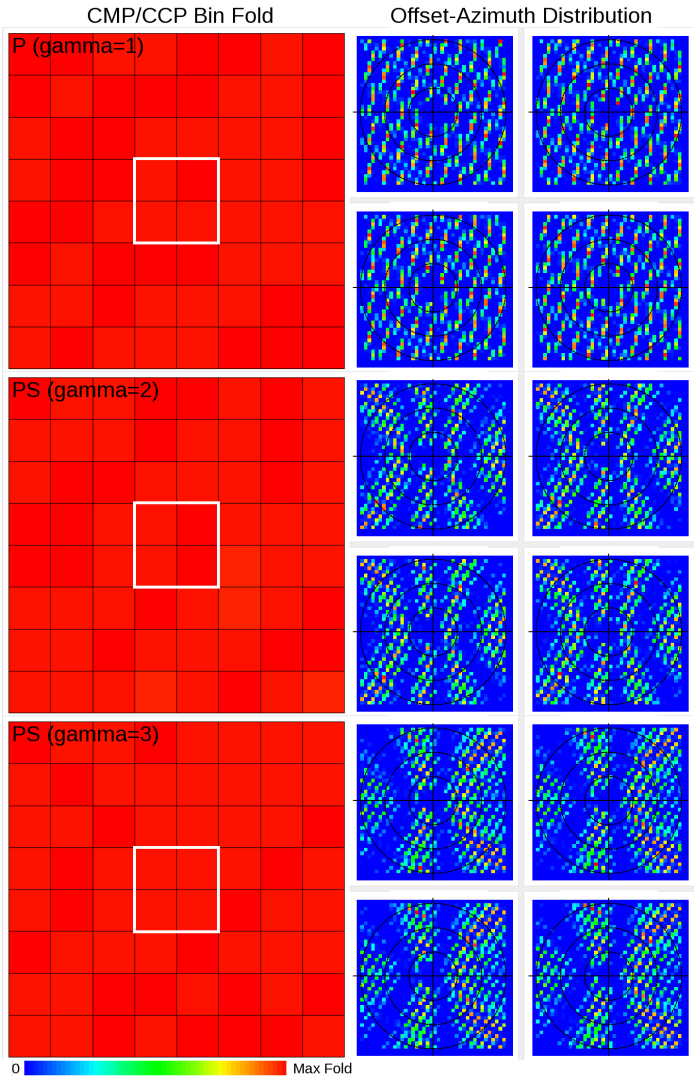

Figure 13: Non-orthogonal parameters as used in the real survey. Geometry: Non-orthogonal 60° as per Figure 12, Source 30m x 30m, Receivers 15m x 30m, Bin 15m x 30m, Target depth 100m.

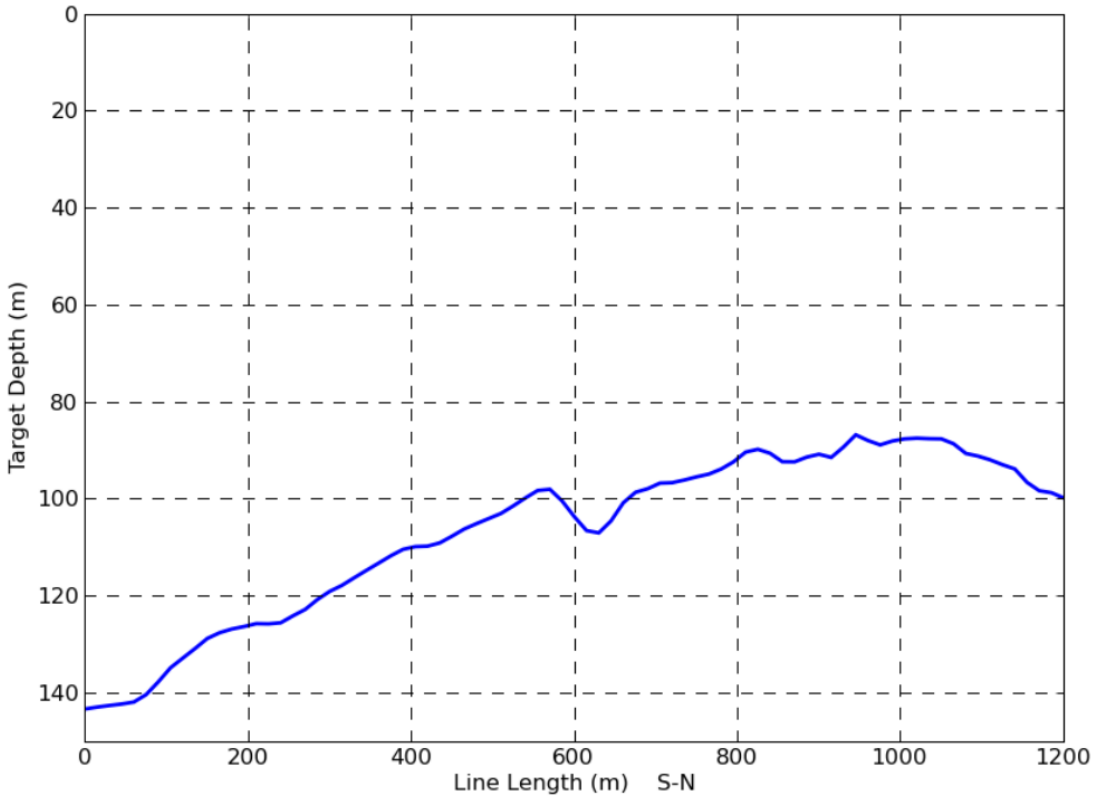

Figure 14: Depth to the target coal seam, estimated from horizon picks on a 2D seismic line previously acquired at this location.

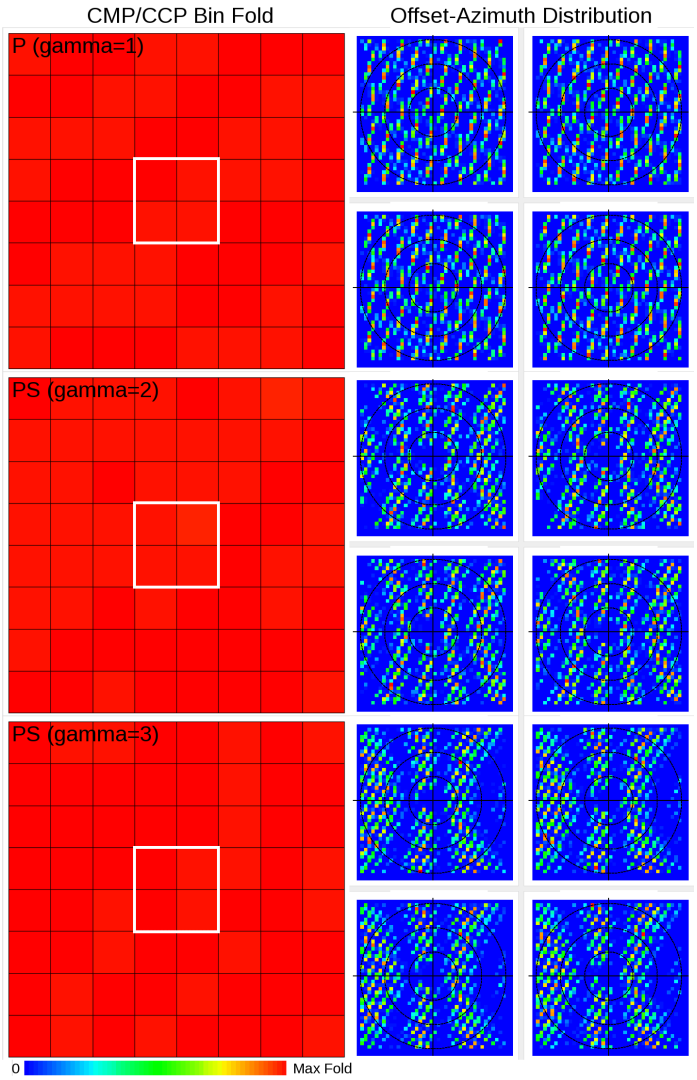

Figure 15: Representative design comparison for changing target depth. Compare to Figure 13. Geometry: Non-orthogonal 60°, Source 30m x 30m, Receivers 15m x 30m, Bin 15m x 30m, Target depth 140m.

For a PS reflection, this equation relates the relative depth R to the relative offset C. It is useful in comparative geometrical analysis of PS reflection surveys at different scales (e.g. petroleum, coal).